Copy No.

RESTRICTED

RM No. L7K13

NACA

RESEARCH MEMORANDUM

WIND-TUNNEL INVESTIGATION OF THE LOW-SPEED STABILITY AND CONTROL CHARACTERISTICS OF A MODEL WITH A SWEPTBACK VEE TAIL AND A SWEPTBACK WING

By

Edward C. Polhamus

Langley Memorial Aeronautical Laboratory
Langley Field, Va.

NATIONAL ADVISORY COMMITTEE FOR AERONAUTICS
WASHINGTON
May 25, 1948

RESTRICTED

NACA RM No. L7K13 RESTRICTED

NATIONAL ADVISORY COMMITTEE FOR AERONAUTICS

RESEARCH MEMORANDUM

WIND-TUNNEL INVESTIGATION OF THE LOW-SPEED STABILITY AND CONTROL CHARACTERISTICS OF A MODEL WITH A SWEPTBACK VEE TAIL AND A SWEPTBACK WING

By Edward C. Polhamus

SUMMARY

Tests were made in the Langley 300 MPH 7- by 10-foot tunnel of a complete model with a sweptback vee tail and a sweptback wing to determine its low-speed stability and control characteristics.

Comparisons were made with the results of tests of the same tail panel with zero dihedral (horizontal tail) on the same wing-fuselage combination.

For a sweptback vee tail it appears that the variation of stabilizer and elevator effectiveness with tail dihedral can be predicted satisfactorily from isolated vee-tail theory. The vee-tail contribution to longitudinal stability, however, is greater than that predicted by isolated vee-tail theory because of the favorable effect of sidewash at the tail. Although it has been found in a previous investigation that this sidewash effect can be estimated for a straight wing, for a highly swept wing this effect appears to be much greater and at present cannot be estimated because of the limited knowledge concerning the flow field behind swept wings.

For the same contribution to stability a vee-tail configuration similar to the one tested will probably require less area than a conventional tail assembly (horizontal and vertical tail).

INTRODUCTION

Interest has been displayed in vee tails because of the possibility of (1) reducing the over-all drag of the empennage, because of a possible reduction in the area required, and (2) locating the tail out of the wing wake without encountering difficult structural problems.

The data of reference 1 indicate that an unswept vee tail behind an unswept wing will require, for the same stability, less area than the combined horizontal and vertical areas of a conventional tail. In view of the interest in swept wings and tails for high-speed flight and inasmuch as there is little data available on the aerodynamic behavior of swept vee tails, an investigation was made of a complete model equipped with a 40° sweptback wing and a 40° sweptback vee tail. The results were compared with the results obtained with the same tail panel at zero tail dihedral (horizontal tail) on the same wing-fuselage combination (reference 2).

SYMBOLS

The system of axes used for the presentation of the data, together with an indication of the sense of the positive forces and moments, is presented in figure 1. Pertinent symbols are defined as follows:

C_L	lift coefficient $\left(\frac{\text{Lift}}{qS}\right)$
C_D	drag coefficient $\left(\frac{\text{Drag}}{qS}\right)$
C_m	pitching-moment coefficient $\left(\frac{M_{cg}}{qS\bar{c}}\right)$
C_l	rolling-moment coefficient $\left(\frac{L}{qSb}\right)$
C_n	yawing-moment coefficient $\left(\frac{N}{qSb}\right)$
C_Y	lateral-force coefficient $\left(\frac{Y}{qS}\right)$
L	rolling moment, foot-pounds
N	yawing moment, foot-pounds
Y	lateral force, pounds
M_{cg}	pitching moment about center of gravity at 26 percent M.A.C.
q	dynamic pressure, pounds per square foot $\left(\rho\frac{V^2}{2}\right)$

q_c impact pressure, pounds per square foot $\left(qf_c\right)$

ρ mass density of air, slugs per cubic foot

V free-stream velocity, feet per second

M Mach number

$f_c = 1 + \left(\frac{1}{4}\right)M^2 + \left(\frac{1}{40}\right)M^4 + \left(\frac{1}{1600}\right)M^6 + \ldots$

S wing area, square feet

$\bar{c}$ wing mean aerodynamic chord (M.A.C.), feet

b wing span, feet

α angle of attack of fuselage center line, degrees

ψ angle of yaw, degrees

ϵ angle of downwash, degrees

ϵ_e effective angle of downwash, degrees

i_t stabilizer setting, measured in plane of symmetry, degrees

δ_e elevator deflection, measured in plane normal to tail quarter-chord line, degrees

δ_r rudder deflection, measured in plane normal to tail quarter-chord line, degrees

δ_f wing trailing-edge flap deflection, degrees

δ_{f_n} wing nose flap deflection, degrees

Γ_t tail dihedral angle, degrees

K ratio of sum of lifts obtained by equal and opposite changes in angle of attack of two semispans of tail to lift obtained by an equal change in angle of attack for complete tail (See reference 3.)

Subscripts:

t tail

α, ψ, δ_e, δ_r, i_t denote partial derivatives with respect to α, ψ, δ_e, δ_r, and i_t $\left(\text{example: } C_{m_\alpha} = \frac{\partial C_m}{\partial \alpha}\right)$

MODEL AND APPARATUS

A three-view drawing of the model as tested is presented in figure 2; details of the tail panel are presented in figure 3. This is the same tail panel that was used for the horizontal tail in the investigation reported in reference 2. Figure 4 shows the vertical position of the vee tail and the three vertical positions of the horizontal tail (all the tails had the same tail length). Figure 5 shows the assumed effective area of the dorsal trunk upon which the vee tail was mounted. All flaps and control surfaces were 20-percent-chord plain flaps except for the nose flaps, which were 15-percent-chord plain flaps.

The tests were conducted in the Langley 300 MPH 7- by 10-foot tunnel. This tunnel is a closed rectangular tunnel of the return-flow type with a contraction ratio of 14 and is powered by a 1600-horsepower synchronous motor.

TESTS AND RESULTS

Test Conditions

Tests of the model in both the cruising and the landing configurations were run at a dynamic pressure of 40 pounds per square foot corresponding to a Mach number of about 0.16. The test Reynolds number was approximately 2.15×10^6, based on a chord of 1.846 feet. The degree of turbulence of the tunnel is not known quantitatively but is believed to be small because of the high contraction ratio.

Corrections

Tares were not applied to the data inasmuch as they were considered negligible. Jet-boundary corrections were computed as follows (reference 4). The subscript M refers to the measured values.

$$\alpha = \alpha_M + 1.42C_{L_M}$$

$$C_D = C_{D_M} + 0.0203C_{L_M}^2$$

$$C_m = C_{m_M} + 0.010C_{L_M}$$

Although reference 4 deals only with unswept wings, an unpublished analysis of the corrections for reflection-plane models mounted vertically in 7- by 10-foot closed rectangular tunnels indicates that, for wings of the same area and span, sweep angles up to 60° have little effect on the corrections.

The dynamic pressure was corrected for blocking as follows:

$$q = 1.02\left(\frac{q_c}{f_c}\right)$$

where $\left(q_c/f_c\right)$ is the dynamic pressure uncorrected for blocking. (See reference 5.) An increment in drag coefficient has been added to account for the horizontal buoyancy effected by the longitudinal static-pressure gradient in the tunnel.

Presentation of Results

An outline of the figures presenting the results is given below:

	Figure nos.
I. Basic Data	
A. Aerodynamic characteristics in pitch	6 to 8
B. Aerodynamic characteristics in yaw	9
C. Neutral points	10
D. Downwash at tail	11

II. Summary Data

	Figure nos.
A. $\left(C_{m_\alpha}\right)_t$ versus Γ_t	12
B. ϵ_{e_α} and $\left(1-\epsilon_{e_\alpha}\right)$ versus tail height	13
C. $C_{m_{i_t}}$ and $C_{m_{\delta_e}}$ versus Γ_t	14
D. $\left(C_{n_\psi}\right)_t$ versus Γ_t	15
E. $C_{n_{\delta_r}}$ versus Γ_t	16

DISCUSSION

Longitudinal Stability Characteristics

Neutral points for the complete model with the vee tail were determined from stabilizer tests (fig. 7), and are presented in figure 10. Also presented are the neutral points for the complete model with a horizontal tail located at three different heights (reference 2). As would be expected, since the vee and horizontal tails had identical panels, the vee tail contributed less longitudinal stability than the horizontal tail; however, the decrease is not so great as that indicated by the isolated tail theory of reference 3.

Figure 12 shows the theoretical variation of the tail contribution to longitudinal stability with dihedral angle for three different heights of the tail mean aerodynamic chord. (See reference 3.) The values at $\Gamma = 0^\circ$ were obtained from horizontal tail tests at the three different tail heights shown in figure 4. Also presented are the experimental values for the vee tail. By a comparison of the experimental and the theoretical values, it can be seen that the vee-tail contribution to longitudinal stability is approximately 40 percent greater than would be expected from the theory. It will be shown in the following section that this increase is due to the favorable effect of sidewash at the tail.

Downwash at the Tail

The curves of the average effective downwash angles for the vee tail and conventional tails (reference 2) are presented in figure 11 for comparison. The term "effective" is applied to the downwash because it was evaluated from pitching-moment data which, for the vee tail, was affected by both the downwash and sidewash associated with the wing vortex wake. The effective downwash may be defined as those downwash angles which, alone, would produce the same effect on longitudinal stability as the combined effects of the actual downwash and sidewash.

For a conventional horizontal tail the sidewash has no effect on the effective angle of attack of the tail. For the vee tail, however, the sidewash will have an effect as illustrated by figure 17.

The lift of a vee tail is determined by the angle of attack in the plane normal to the chord plane. However, this angle is reduced not by the normal component of the downwash angle (as was assumed in reference 3) but by the normal component of the resultant angle. As is shown in figure 17, the normal component of the resultant angle is less than that of the downwash angle by an amount equal to the normal component of the sidewash angle. The effect of sidewash is to increase the angle of attack of the tail or in other words to decrease the effective downwash. It will be noted in figure 17 that the induced velocities rather than the induced angles are shown. For small angles, however, the induced angles are proportional to the induced velocities. Actually the tip vortices of both wing panels should be considered but the one shown, since it is the closest to the point in question, will determine whether or not the sidewash will increase or decrease the effective downwash. The other vortex will tend to decrease this effect, but the net effect will be a decrease in effective downwash.

Verification of the sidewash effect can be obtained by comparing the rate of change of effective downwash angle with fuselage angle of attack obtained with the horizontal tails with that obtained with the vee tail (fig. 11). Values of these slopes in the low lift range are presented in figure 13. The curve showing the effect of tail height on the rate of change of the actual downwash ϵ_{e_α} obtained from the horizontal-tail tests is presented along with the single value of ϵ_{e_α} obtained with the vee tail. The effective tail height of the vee tail is assumed to be equal to the height of the tail mean aerodynamic chord. It will be noted from this figure that the effective rate of change of downwash for the vee tail is approximately 50 percent less than the actual rate of change at the same effective tail height. This effect is apparently caused by the favorable effect of sidewash at the tail. A method of predicting the sidewash effect behind a straight wing is presented in reference 1. However, the sidewash effect behind a sweptback wing appears to be greater than that behind a straight wing and the straight-wing theory underestimates it. A part of this discrepancy is probably due to the fact that behind a swept wing the bound vortex will also induce a sidewash, but the main cause for the discrepancy is that the flow field about a highly swept wing cannot be satisfactorily represented by a lifting line.

The rate of change of effective downwash angle with fuselage angle of attack, obtained with the extended vee-tail panels, is also presented. (See figs. 3 and 4.) This slope is less than that obtained with the normal vee tail because of the higher effective tail height and the increase in sidewash effect with increasing tail span. The sidewash effect increases from zero at the plane of symmetry to a maximum at a spanwise station approximately equal to the wing vortex semispan.

Also presented in figure 13 are values of $\left(1 - \epsilon_{e_\alpha}\right)$ which are proportional to the tail contribution to longitudinal stability. It will be noted that, because of the decrease in the rate of change of effective downwash, the value of $\left(1 - \epsilon_{e_\alpha}\right)$ for the vee tail is approximately 45 percent greater than that for the horizontal tail. This fact indicates that the increase in stability is caused by the favorable effect of sidewash at the tail.

It will be noted in figure 11 that for the vee tail at high angles of attack the rate of change of effective downwash with angle of attack increases rapidly and approaches that obtained with the horizontal tail. This increase is caused by changes in the relative positions of the tail and the vortex sheet. As the tail moves closer to the vortex sheet, the favorable effect of sidewash decreases. At very high angles of attack a part of the tail may be below the sheet, in which case sidewash will have an unfavorable effect on that portion of the tail.

Longitudinal Control Characteristics

Values of stabilizer and elevator effectiveness parameters for tail dihedral angles of 0° and 45° are presented in figure 14. The values at 45° were obtained from figures 6 and 7 while those at 0° were obtained from tests of the same tail panel on the same wing-fuselage combination (reference 2). Also presented in this figure are the theoretical variations of effectiveness with tail dihedral angle, as predicted by the isolated tail theory of reference 3. The close agreement between the theoretical and experimental values of the effectiveness parameters is apparent.

The loss in stabilizer effectiveness associated with deflection of the wing flaps is probably due to a decrease in the dynamic pressure at the tail caused by the flap wake.

Lateral Stability Characteristics

The lateral stability characteristics are presented in figure 9. The negative dihedral in the tail-off cruising configuration (fig. 9(a)) is due to the tip stall associated with sweptback wings at high angles of attack. (See reference 6.)

The tail contribution to directional stability $\left(C_{n_\psi}\right)_t$ obtained from figure 9 is presented in figure 15 along with the theoretical variation with tail dihedral angle, as predicted by the isolated tail theory of reference 3. It will be noted that there is a very large

increase in lateral stability over that predicted by theory. Inasmuch as the tail was not yawed with the fuselage held at zero yaw the rate of change of sidewash with angle of yaw and the tail effectiveness in yaw cannot be determined. A part of the increase in stability may be due to an increase in one or both of these factors. The greater portion of the increase is probably due to the dorsal trunk (fig. 5) which increases not only the area of the tail but the aspect ratio as well. Per unit area, the dorsal trunk produces more yawing moment than the vee tail.

Rudder Control Characteristics

The value of the rudder control parameter $C_{n_{\delta_r}}$ for the vee tail as obtained from figure 9 is presented in figure 16, along with the theoretical variation with tail dihedral angle as predicted by the isolated tail theory of reference 3. It will be noted that the experimental value of $C_{n_{\delta_r}}$ is approximately 33 percent greater than that predicted by theory. A large part of this increase is probably due to the rudder-induced load on the dorsal trunk upon which the tail was mounted. (See fig. 5.)

CONCLUSIONS

Based on low-speed wind-tunnel tests of a complete model with a sweptback vee tail and a sweptback wing, the following conclusions were reached:

1. For a sweptback vee tail, the variation of stabilizer and elevator effectiveness with tail dihedral can be predicted satisfactorily from isolated vee-tail theory.

2. The vee-tail contribution to longitudinal stability is greater than that predicted by isolated vee-tail theory because of the favorable effect of sidewash at the tail. However, the sidewash induced by a swept wing is difficult to estimate because of the limited knowledge concerning the flow field behind sweptback wings.

3. For the same contribution to stability a vee-tail configuration similar to the one tested will probably require less area than a conventional tail assembly (horizontal and vertical tail).

Langley Memorial Aeronautical Laboratory
National Advisory Committee for Aeronautics
Langley Field, Va.

REFERENCES

1. Polhamus, Edward C., and Moss, Robert J.: Wind-Tunnel Investigation of the Stability and Control Characteristics of a Complete Model Equipped with a Vee Tail. NACA TN No. 1478, 1947.

2. Weil, Joseph, Comisarow, Paul, and Goodson, Kenneth W.: Longitudinal Stability and Control Characteristics of an Airplane Model Having a 42.8° Sweptback Circular-Arc Wing with Aspect Ratio 4.00, Taper Ratio 0.50, and Sweptback Tail Surfaces. NACA RM No. L7G28, 1947.

3. Purser, Paul E., and Campbell, John P.: Experimental Verification of a Simplified Vee-Tail Theory and Analysis of Available Data on Complete Models with Vee Tails. NACA ACR No. L5A03, 1945.

4. Gillis, Clarence L., Polhamus, Edward C., and Gray, Joseph L., Jr.: Charts for Determining Jet-Boundary Corrections for Complete Models in 7- by 10-Foot Closed Rectangular Wind Tunnels. NACA ARR No. L5G31, 1945.

5. Thom, A.: Blockage Corrections in a Closed High-Speed Tunnel. R. & M. No. 2033, British A.R.C., 1943.

6. Goodson, Kenneth W., and Comisarow, Paul: Lateral Stability and Control Characteristics of an Airplane Model Having a 42.8° Sweptback Circular-Arc Wing with Aspect Ratio 4.00, Taper Ratio 0.50, and Sweptback Tail Surfaces. NACA RM No. L7G31, 1947.

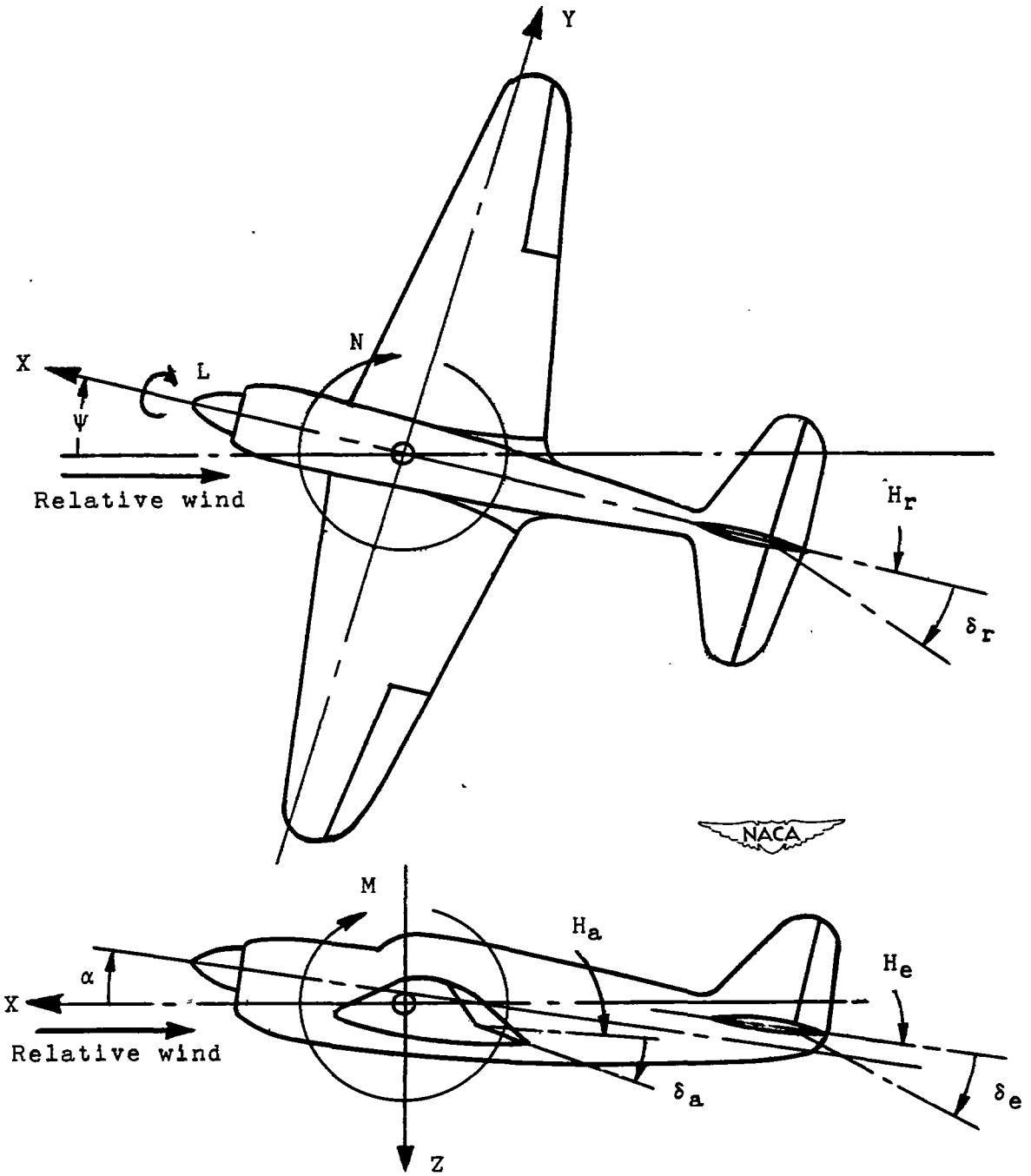

Figure / .- System of axes and control-surface hinge moments and deflections. Positive values of forces, moments, and angles are indicated by arrows. Positive values of tab hinge moments and deflections are in the same directions as the positive values for the control surfaces to which the tabs are attached.

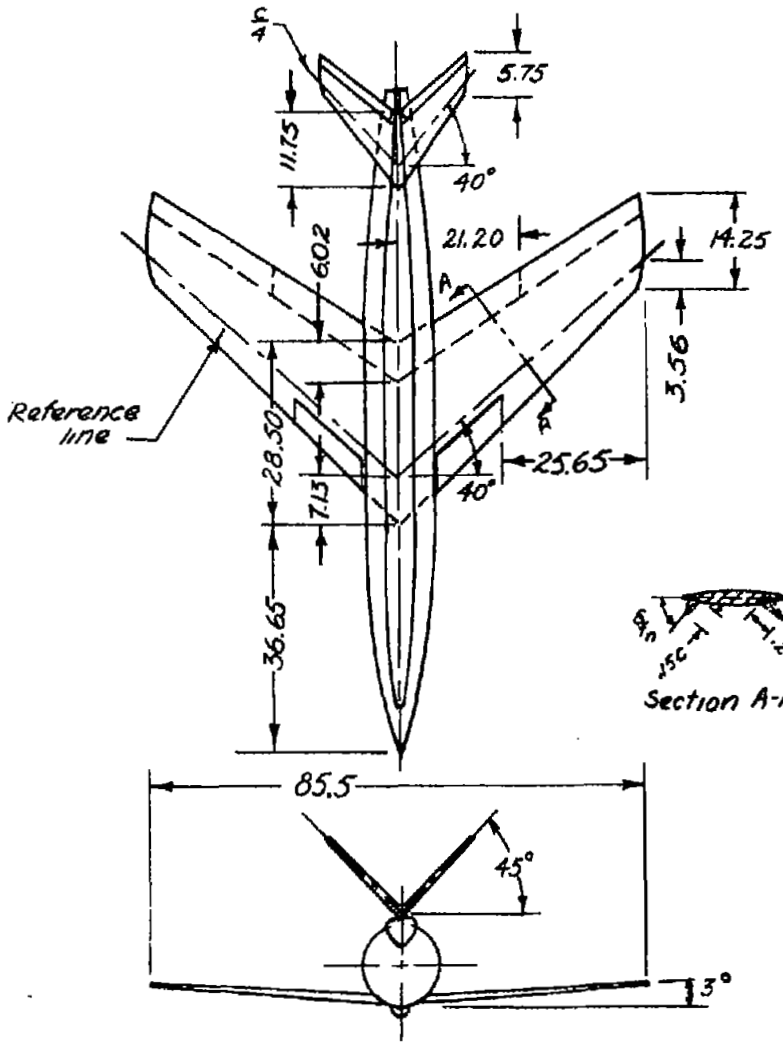

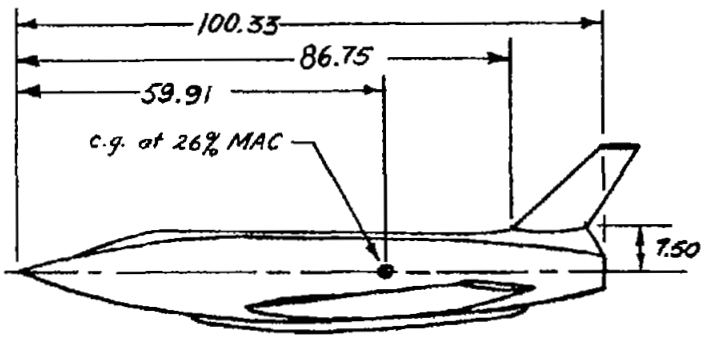

AREAS

	Sq. ft.
Wing (including flaps & fuselage)	12.70
Vee tail (total)	
Original	2.06
Extended	2.41

AIRFOIL

Circular-arc section, 10% thickness (measured perpendicular to wing reference line.)

NACA

Figure 2.-Three-view drawing of the model as tested.

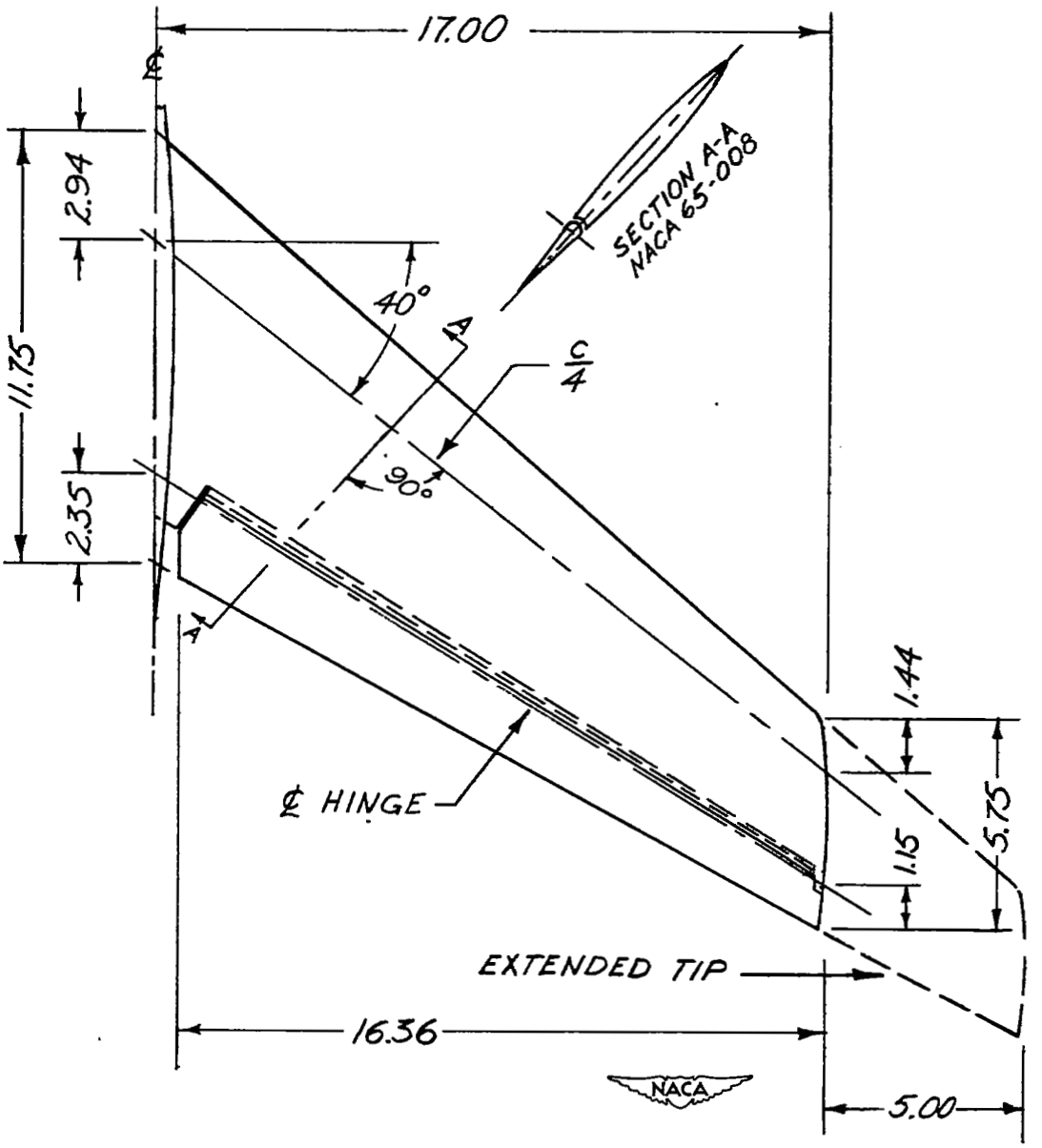

Figure 3.- Drawing of the tail panel.

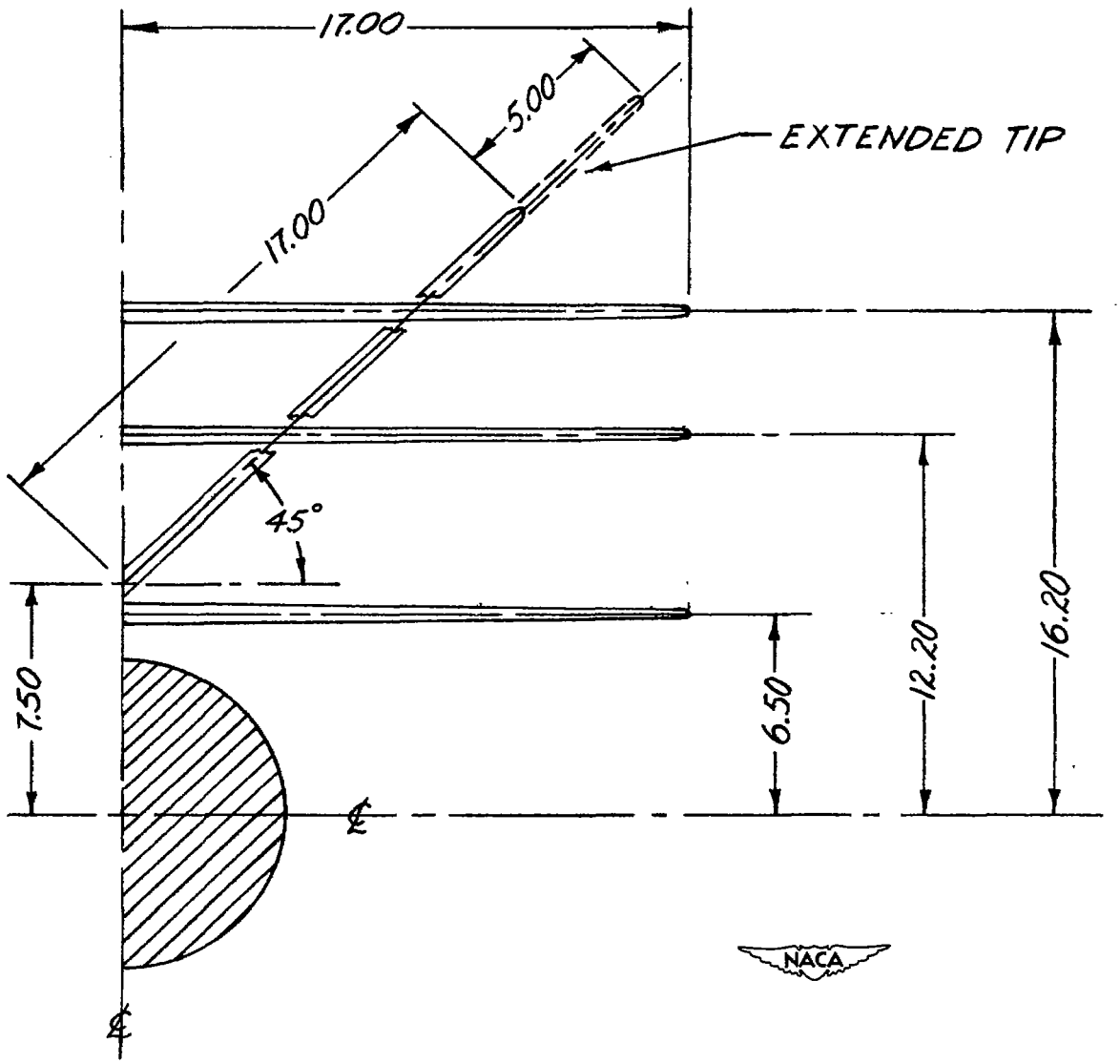

Figure 4.- Drawing showing the various tail positions.

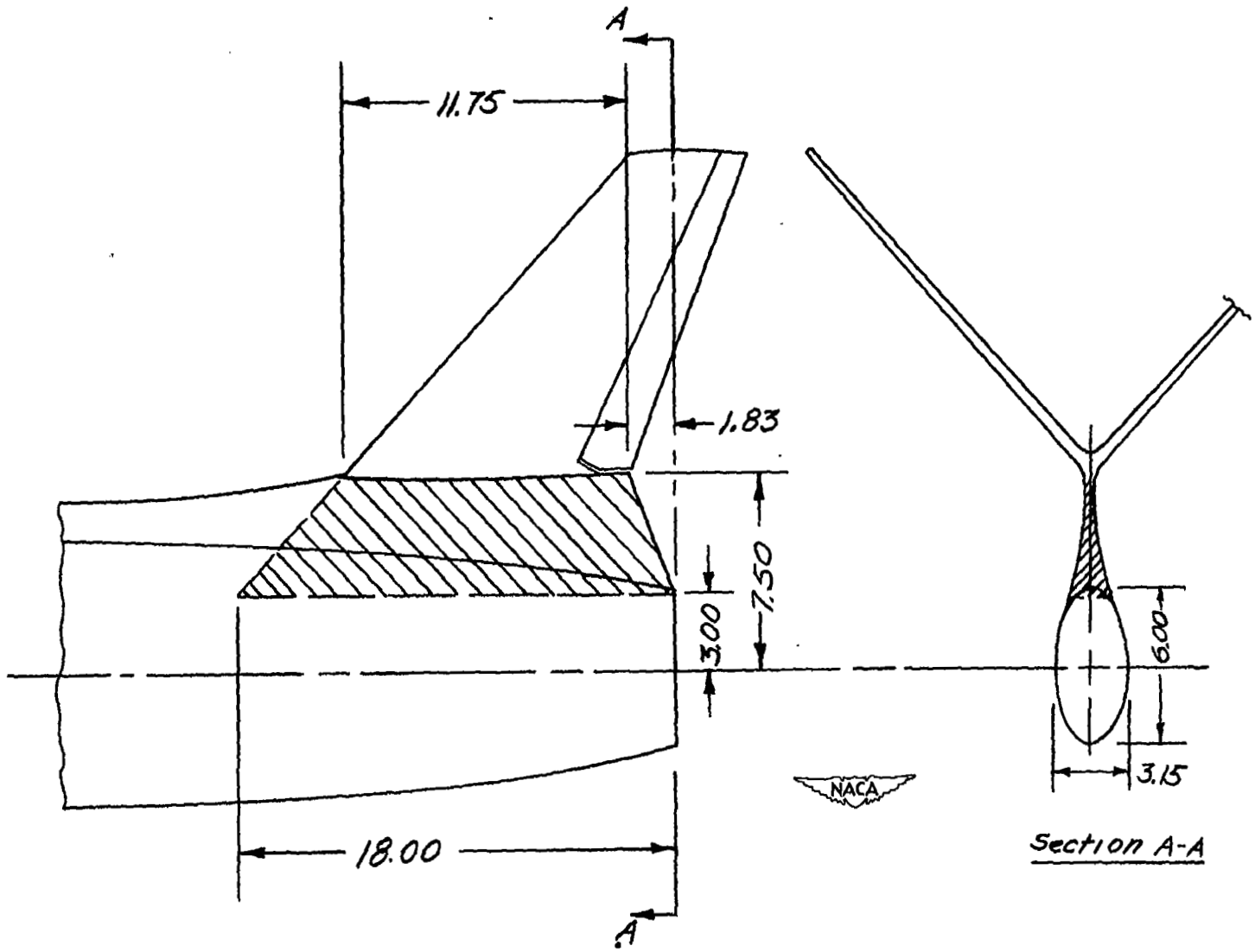

Figure 5.- Details showing probable effective area of dorsal trunk.

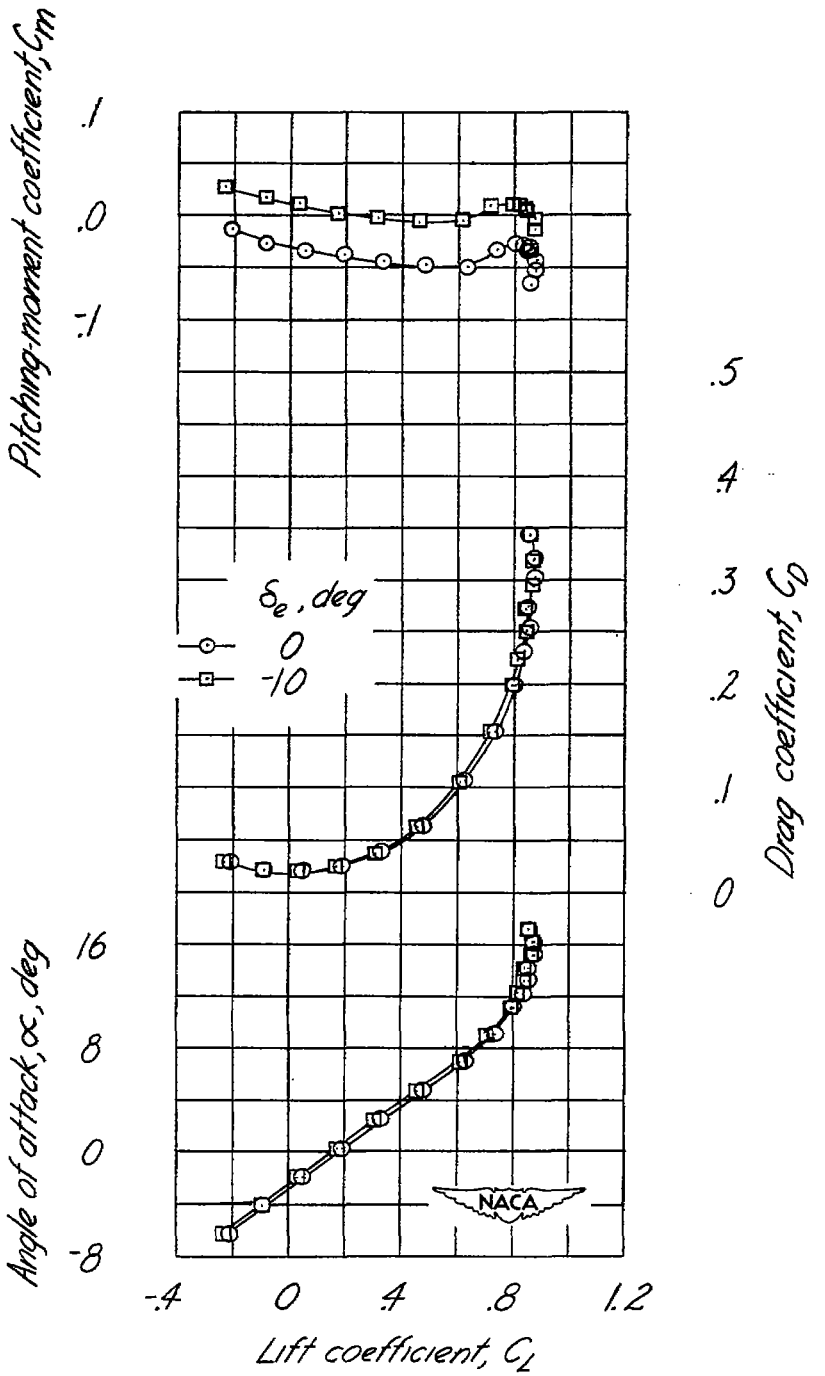

(a) $\delta_f = 0°$, $\delta_{f_n} = 0°$

Figure 6.- Effect of elevator deflection on the aerodynamic characteristics in pitch; $i_t = 5°$.

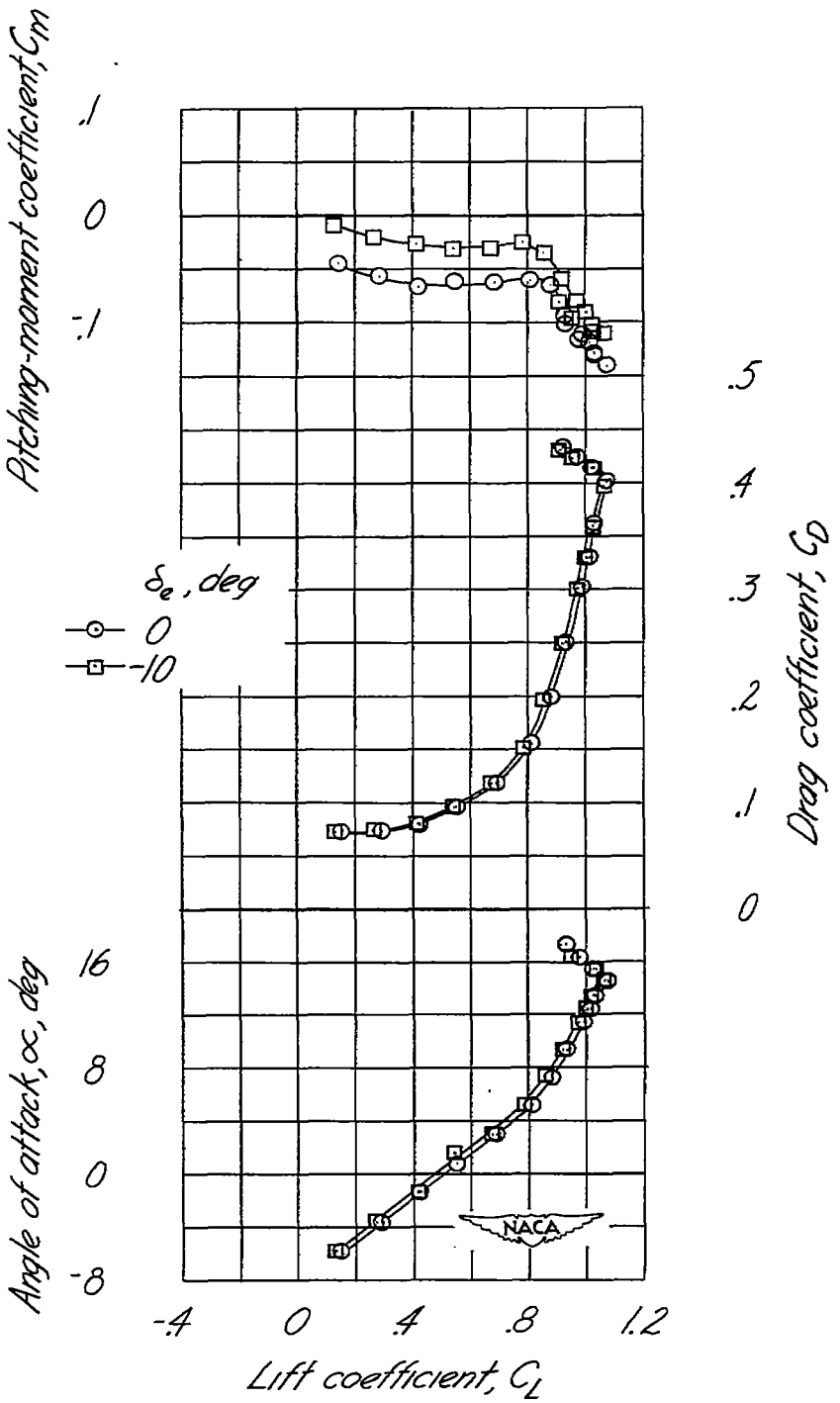

(b) $\delta_f = 50°$, $\delta_{f_n} = 15°$

Figure 6.- Concluded.

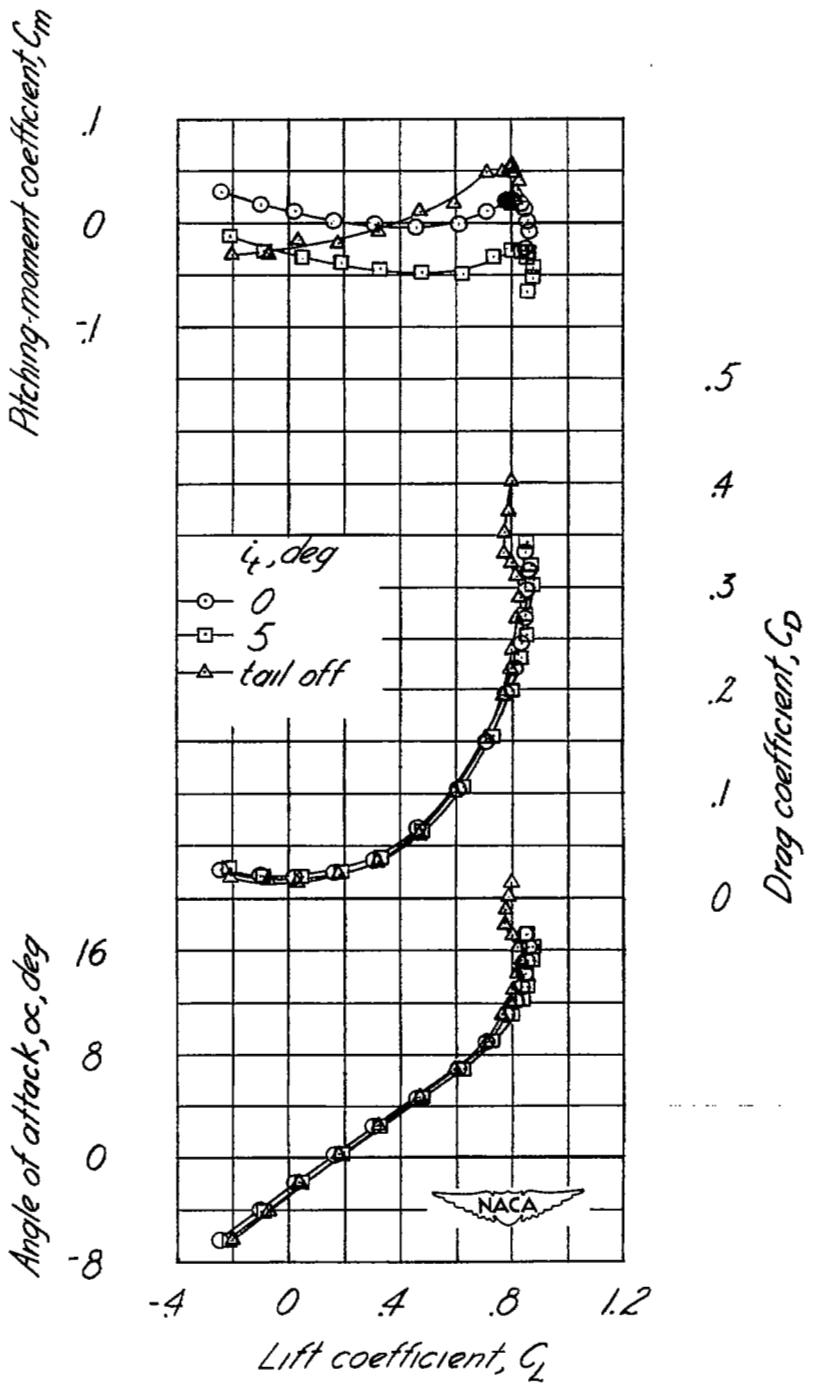

(a) $\delta_f = 0°$, $\delta_{f_n} = 0°$

Figure 7.- Effect of stabilizer setting on the aerodynamic characteristics in pitch; $\delta_e = 0°$.

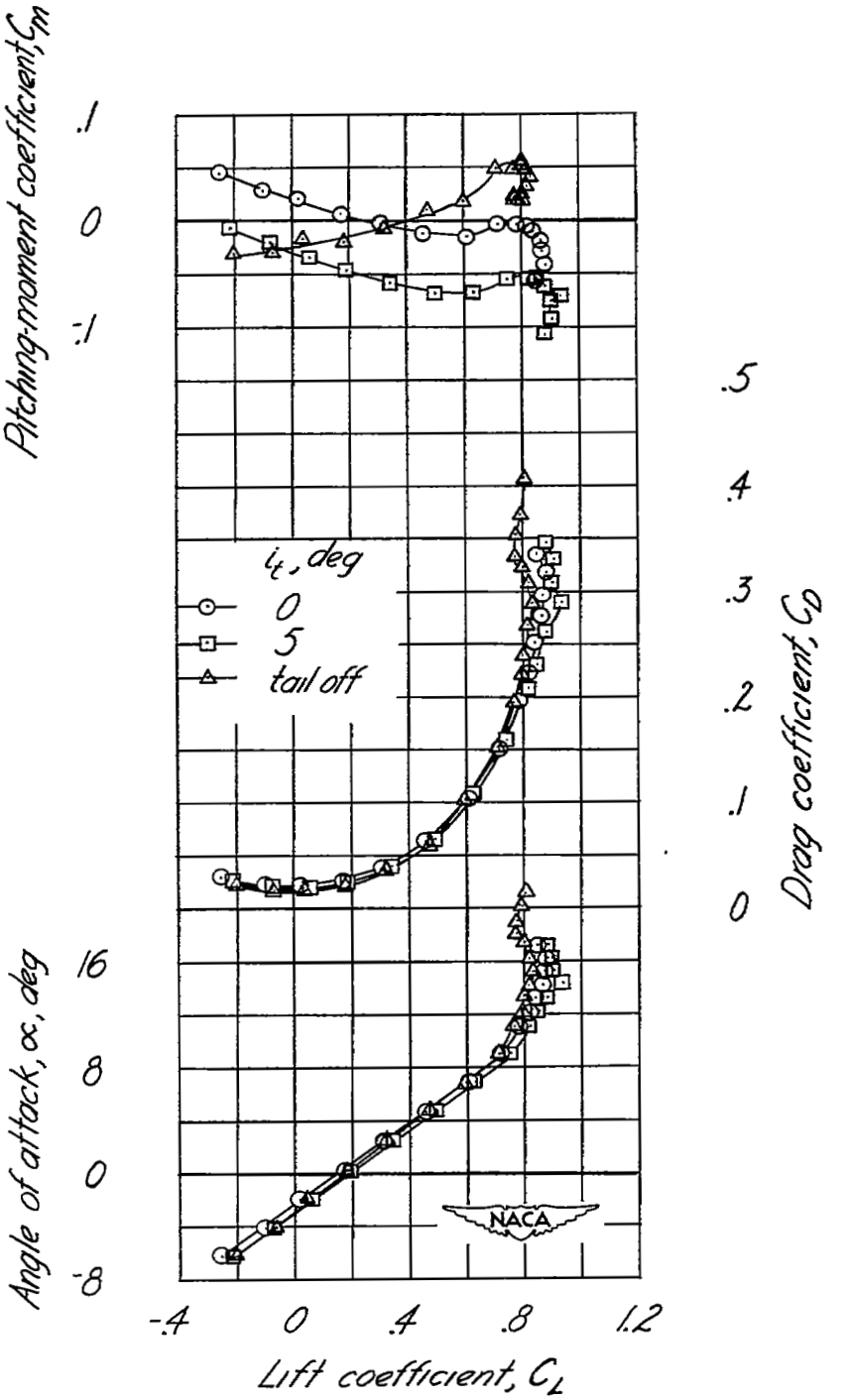

(b) $\delta_f = 0°$, $\delta_{fn} = 0°$, extended tail span

Figure 7.- Continued.

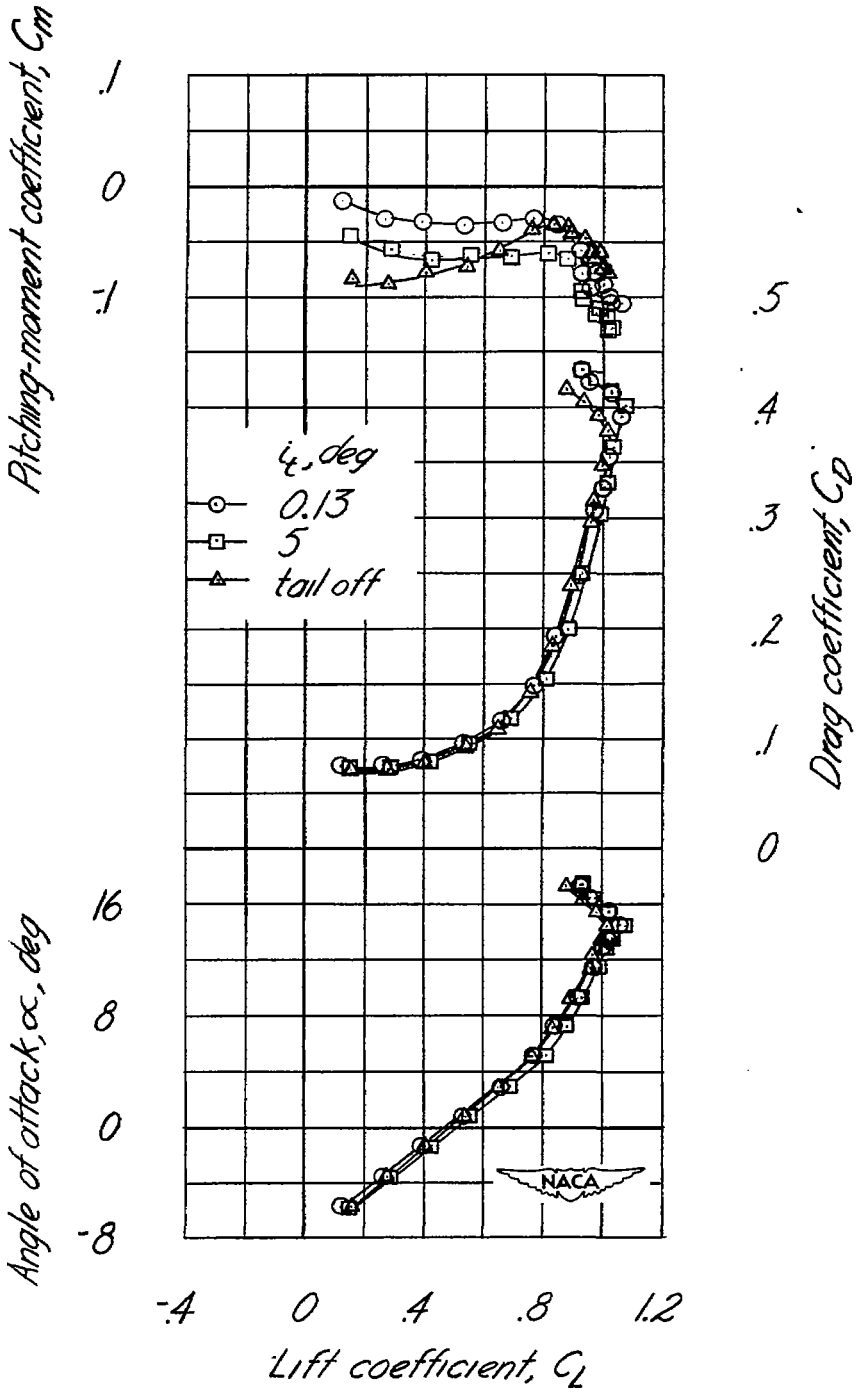

(c) $\delta_f = 50°$, $\delta_{f_n} = 15°$

Figure 7.-Concluded.

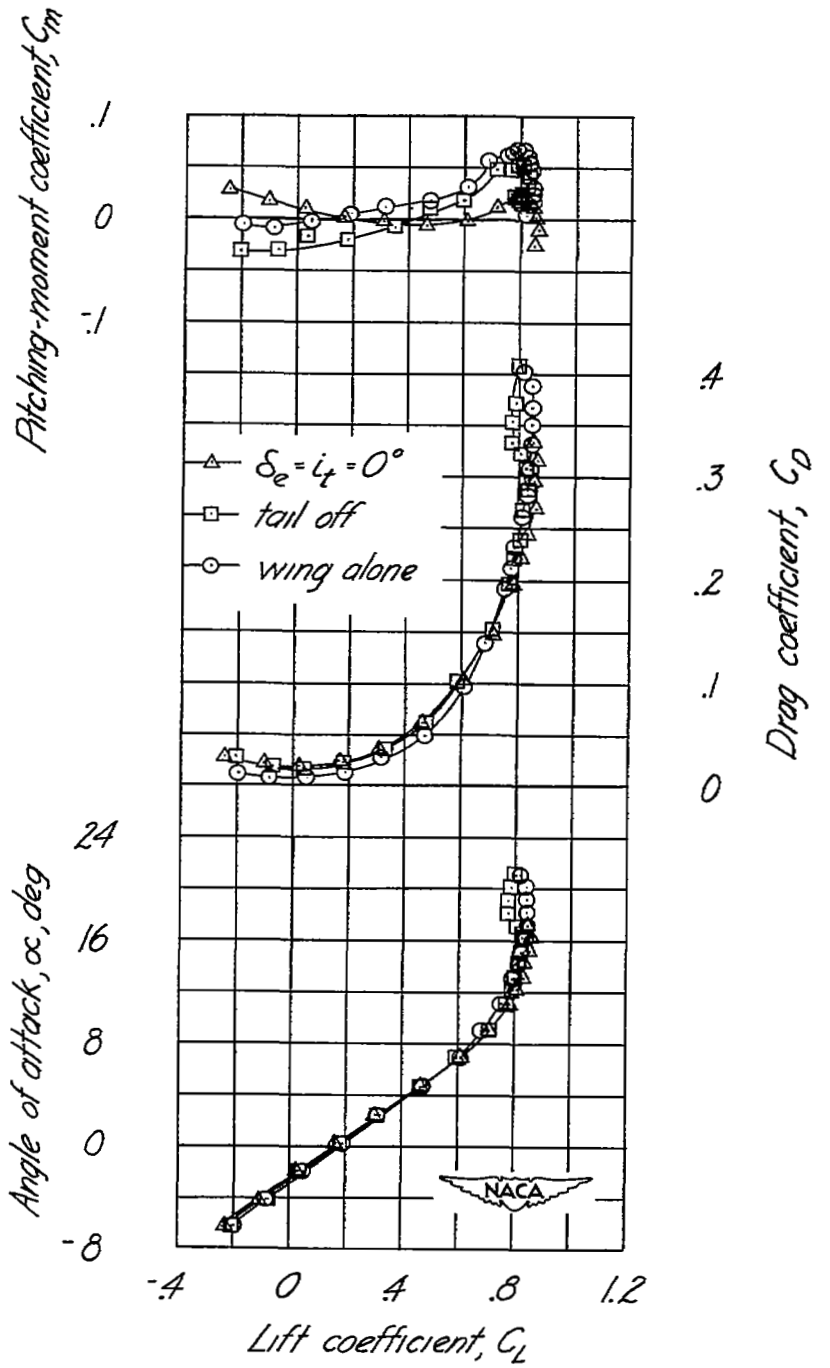

Figure 8. -Effect of component parts on the aerodynamic characteristics in pitch, $\delta_f = 0°$, $\delta_{f_n} = 0°$.

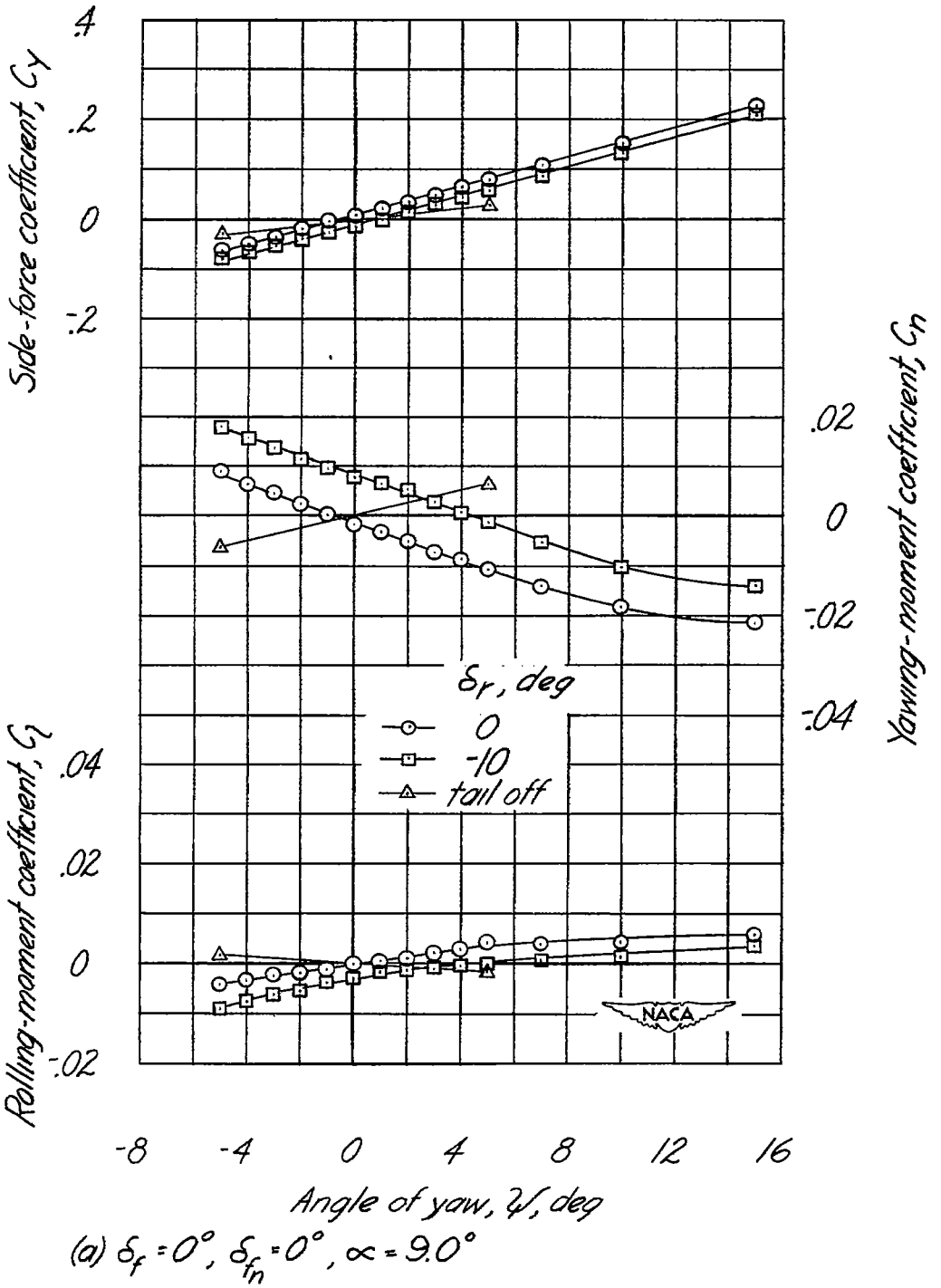

(a) $\delta_f = 0°$, $\delta_{f_n} = 0°$, $\alpha = 9.0°$

Figure 9.- Effect of rudder deflection on the aerodynamic characteristics in yaw.

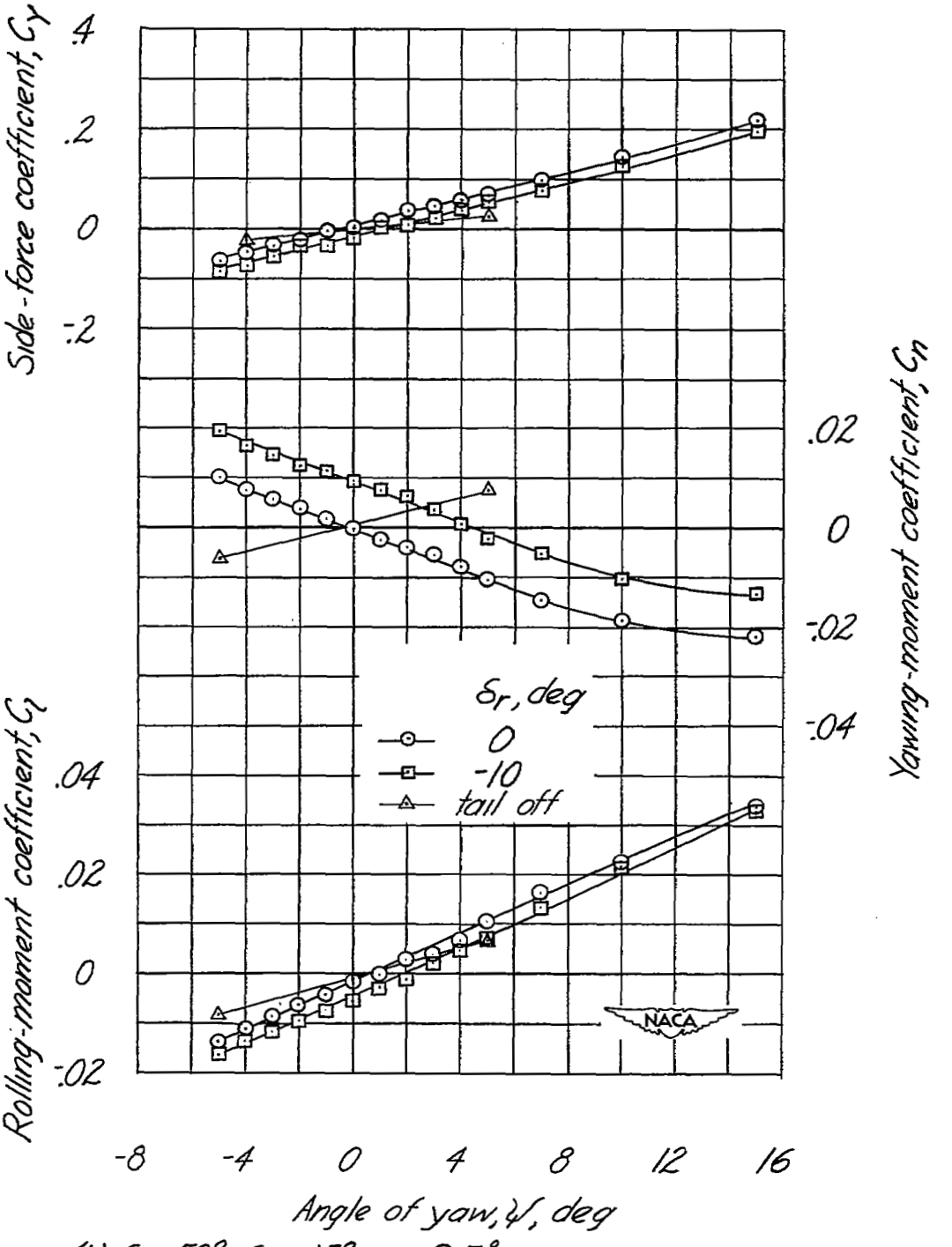

(b) $\delta_f = 50°$, $\delta_{f_n} = 15°$, $\alpha = 9.3°$

Figure 9.- Concluded.

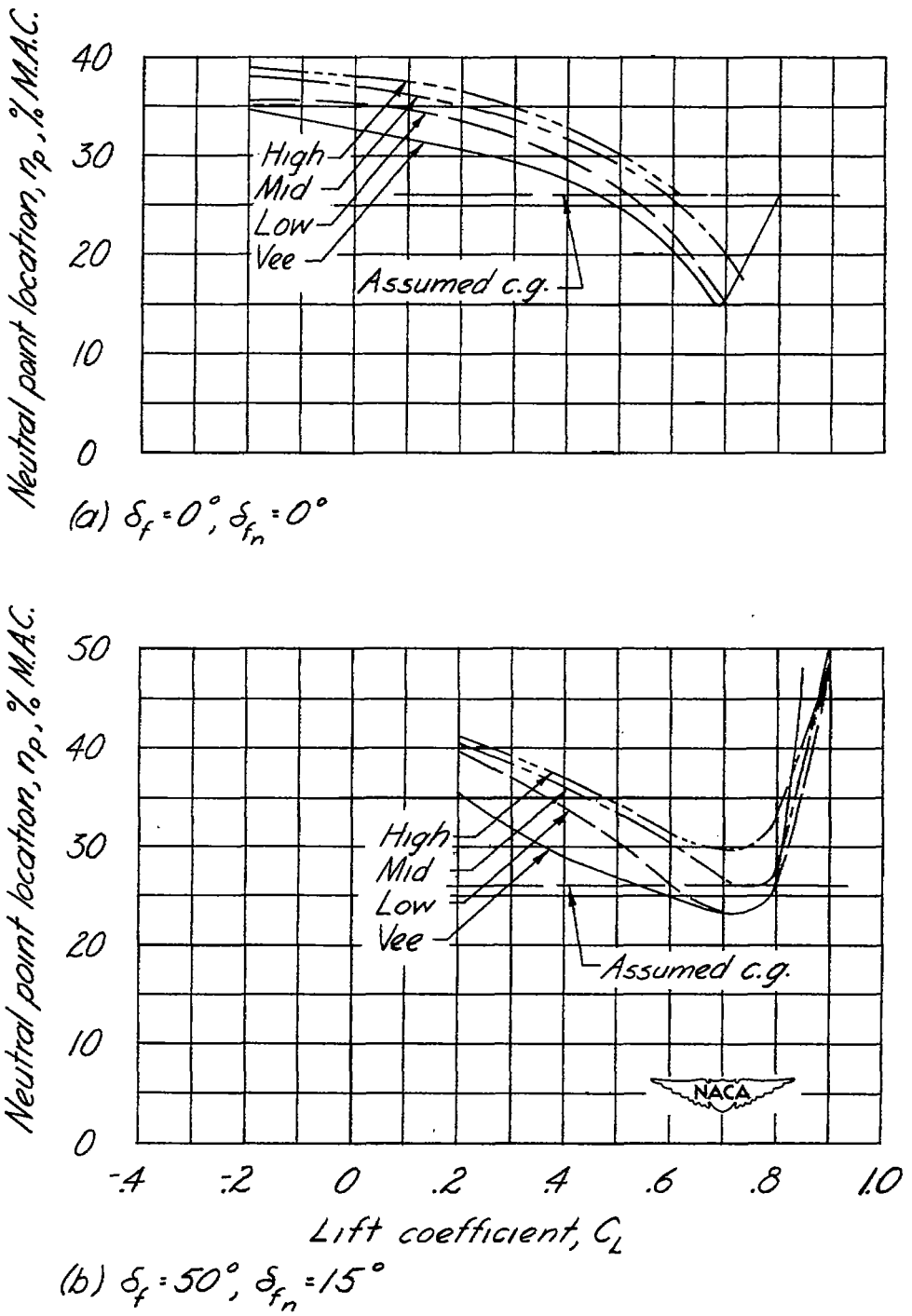

Figure 10.- Variation of neutral-point location with lift coefficient.

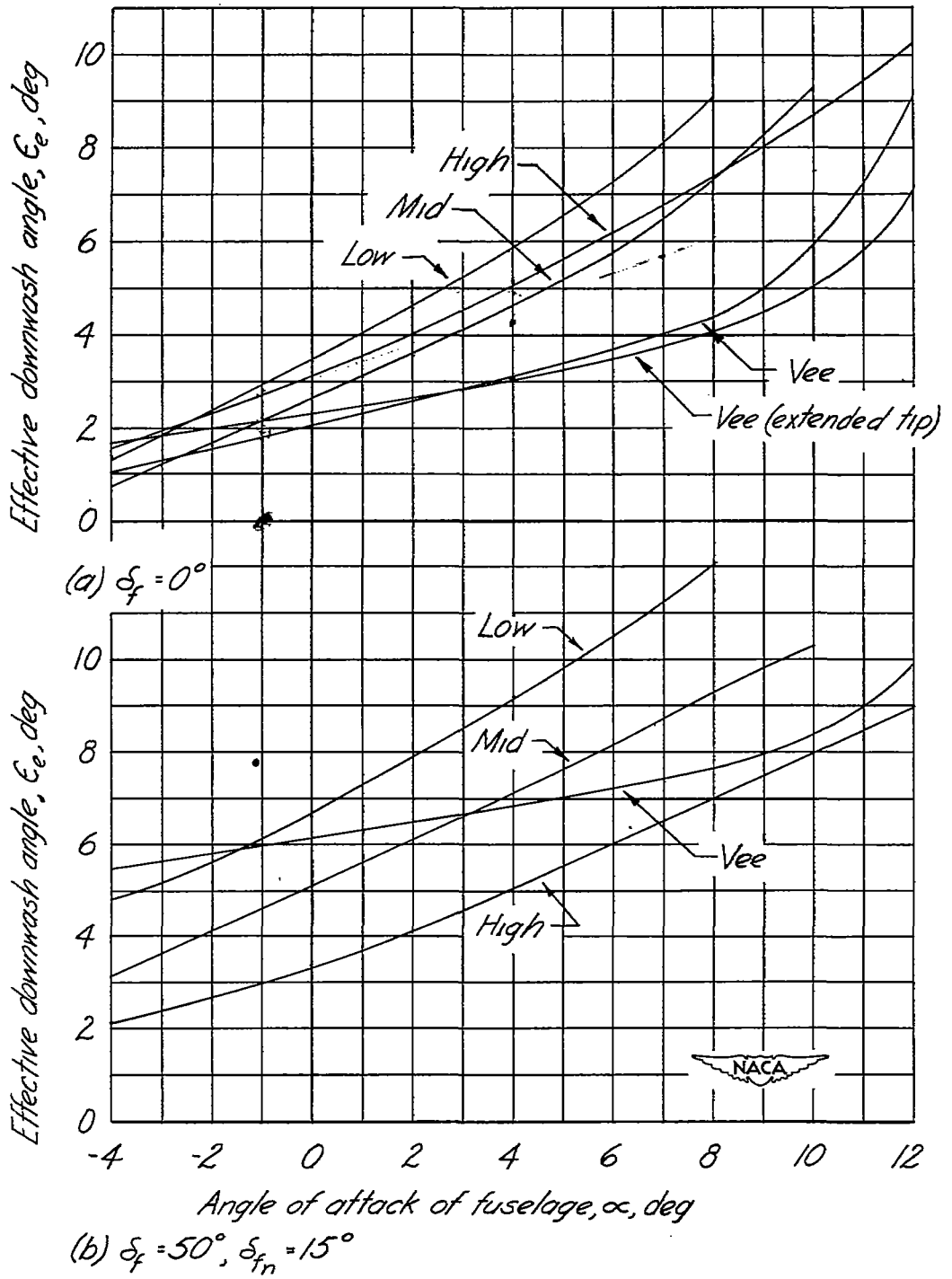

Figure 11.- Variation of effective downwash angle with fuselage angle of attack.

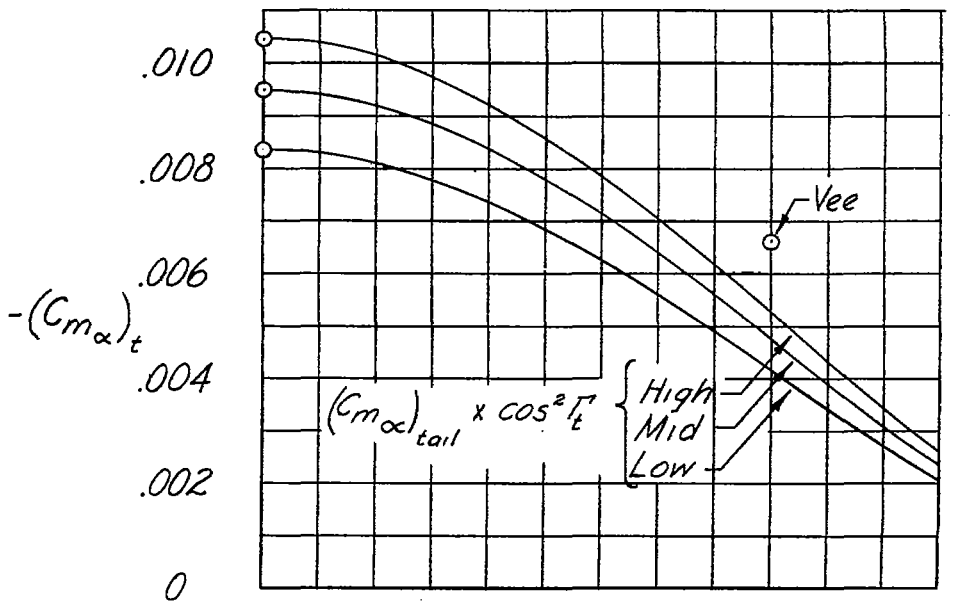

(a) $\delta_f = 0°$, $C_L = 0$

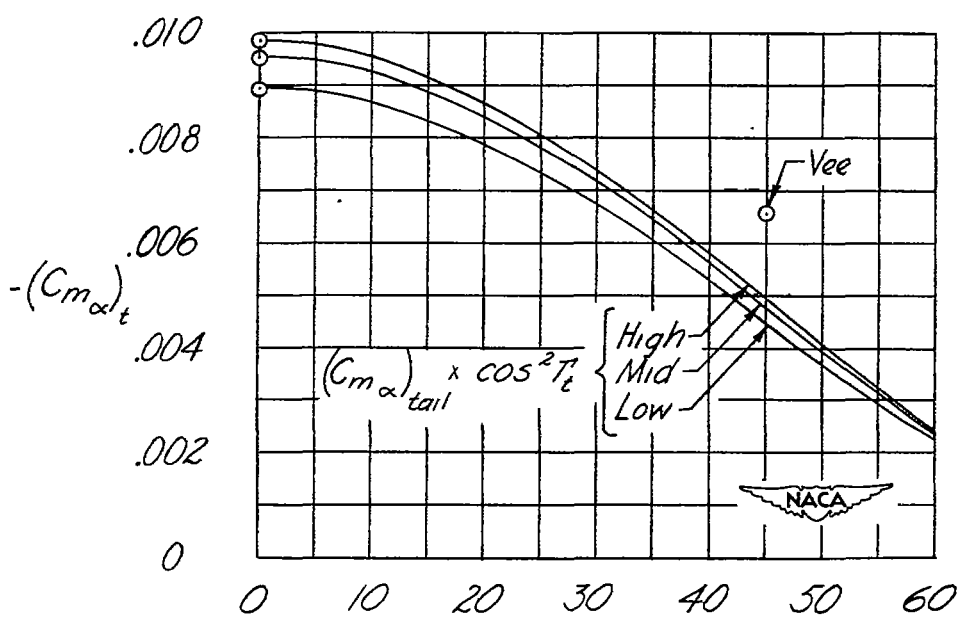

(b) $\delta_f = 50°$, $\delta_{f_n} = 15°$, $C_L = 0.2$

Figure 12.- Effect of tail dihedral angle and tail height on $(C_{m_\alpha})_t$.

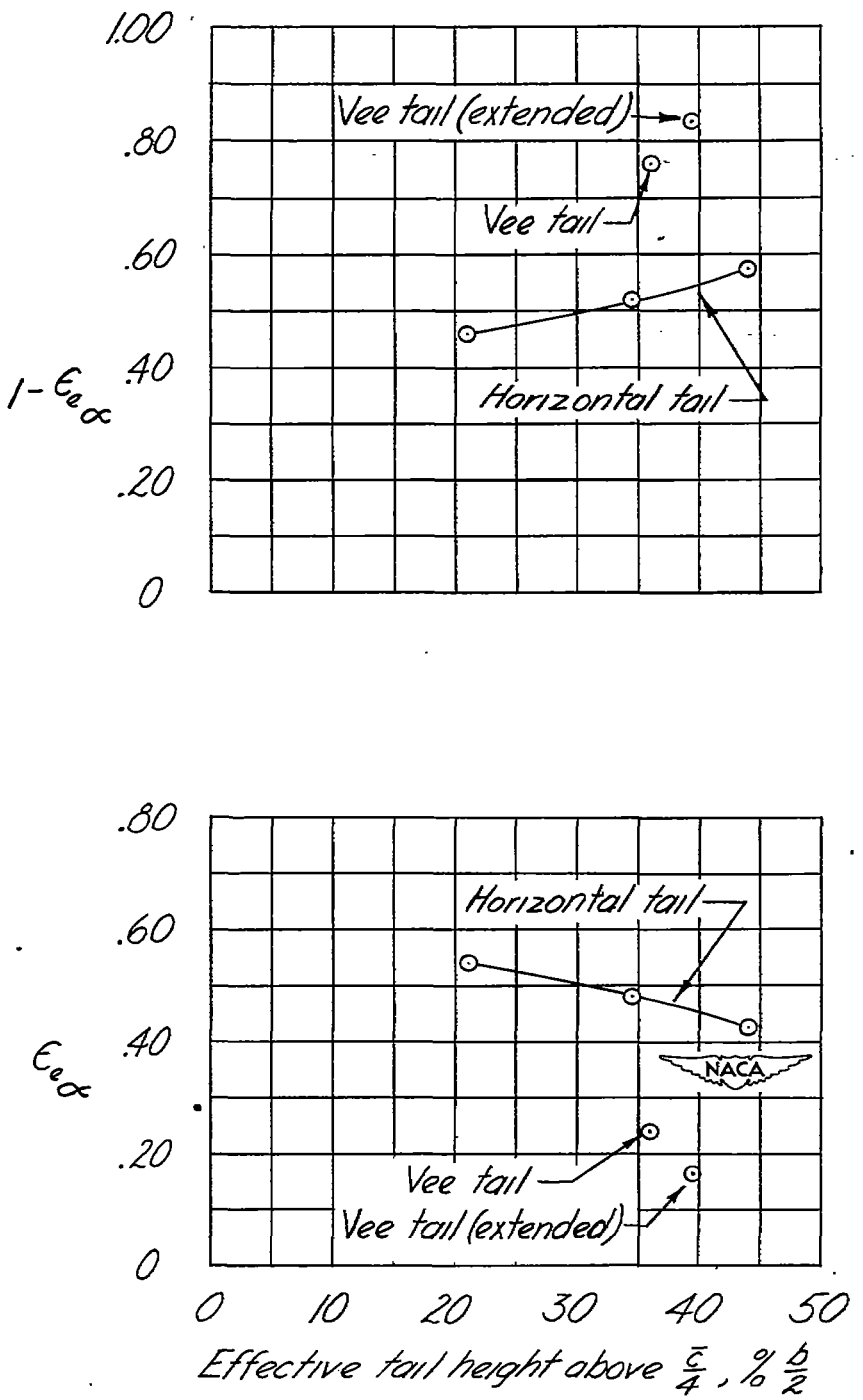

Figure 13. - Variation of ϵ_{e_α} and $1-\epsilon_{e_\alpha}$ with tail height; $\alpha = 0°$.

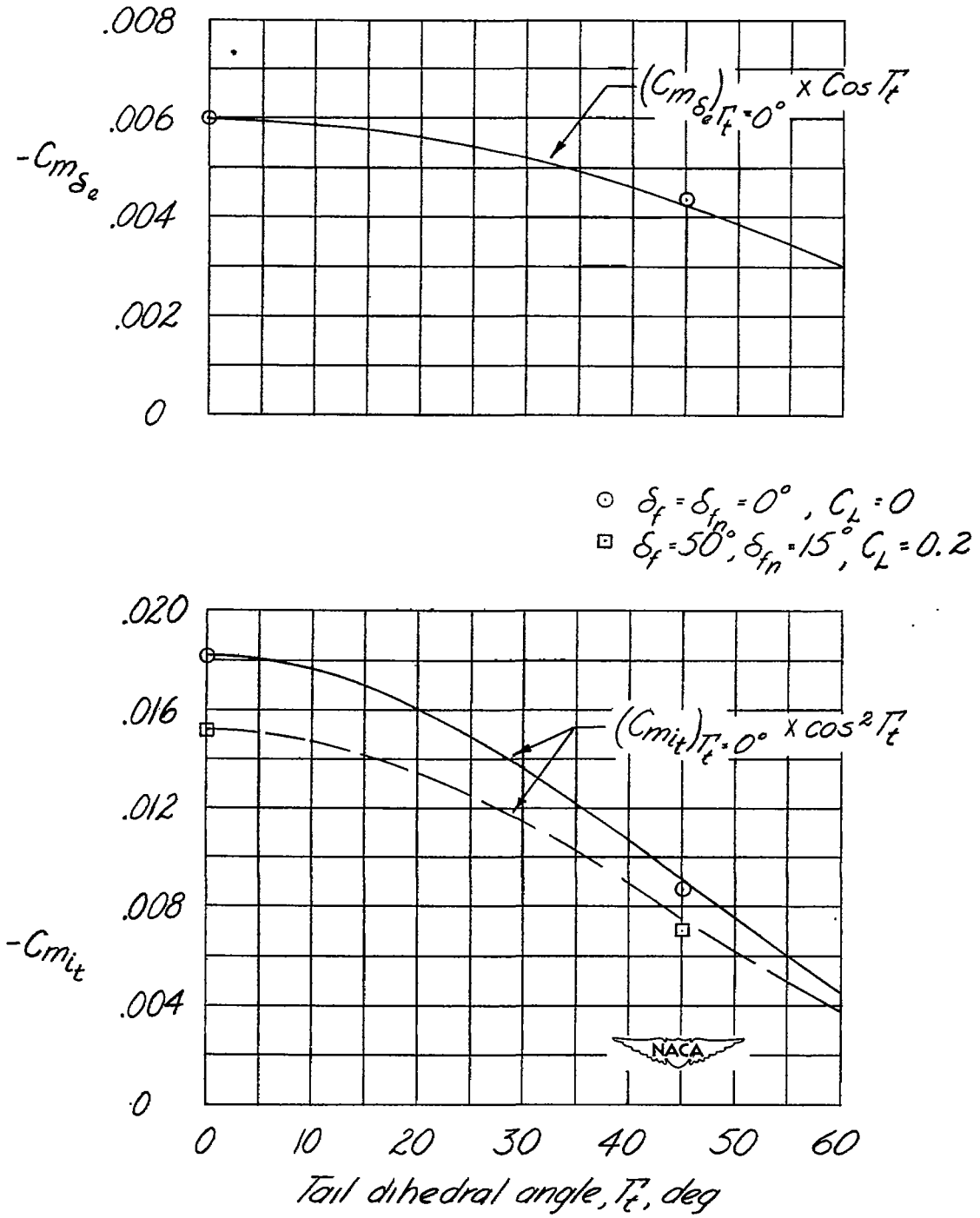

Figure 14.- Effect of tail dihedral angle on $C_{m_{i_t}}$ and $C_{m_{\delta_e}}$.

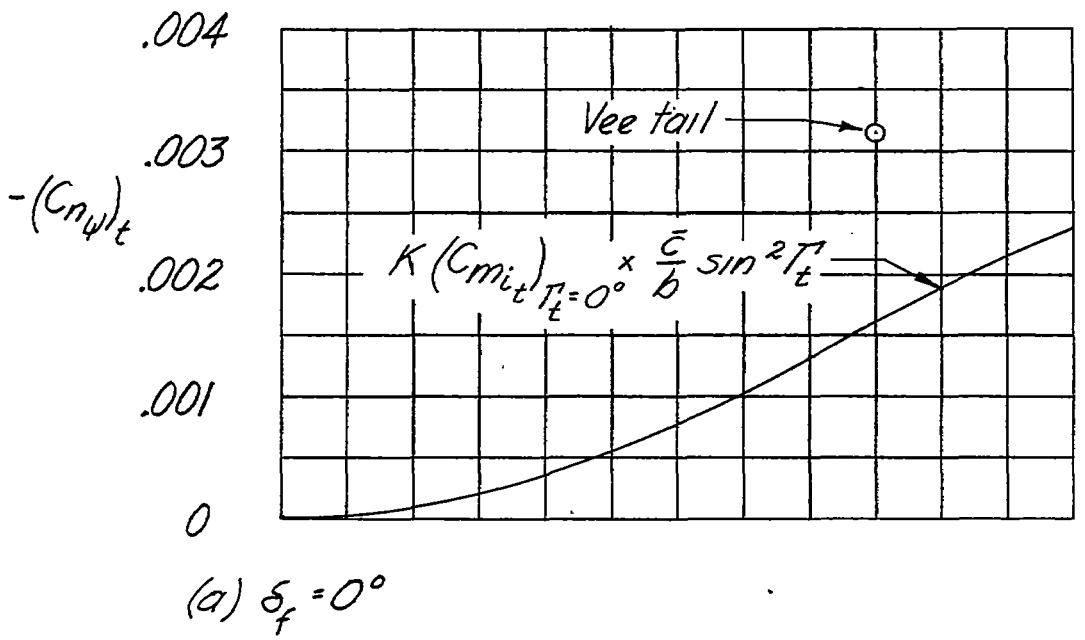

(a) $\delta_f = 0^\circ$

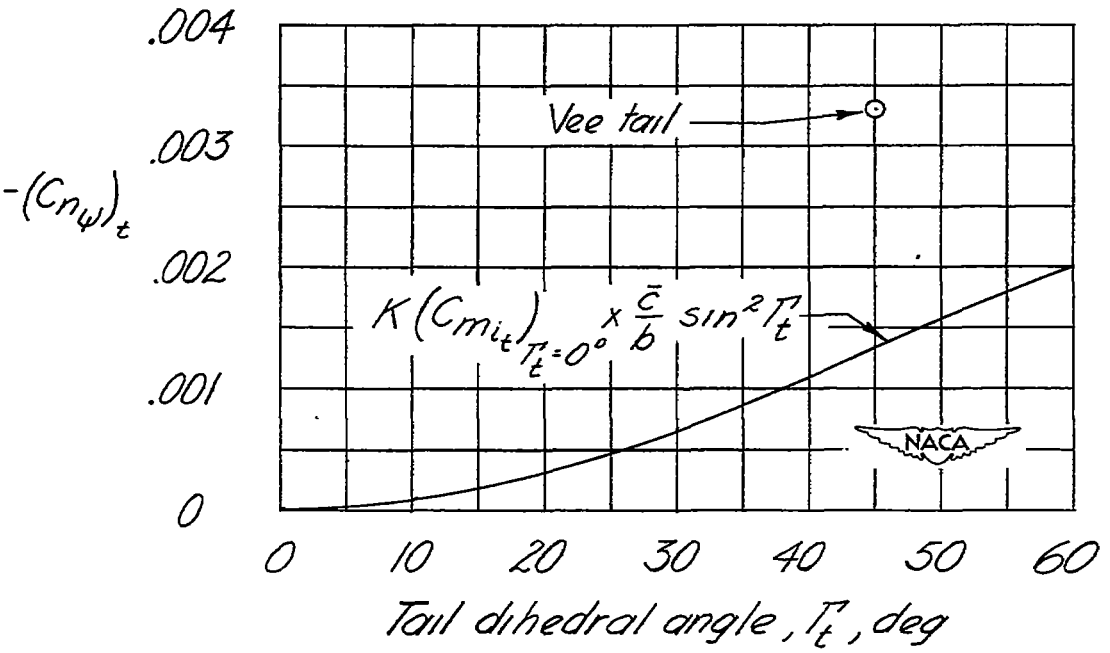

(b) $\delta_f = 50^\circ$, $\delta_{f_n} = 15^\circ$

Figure 15.- Effect of tail dihedral angle on $(C_{n_\psi})_t$.

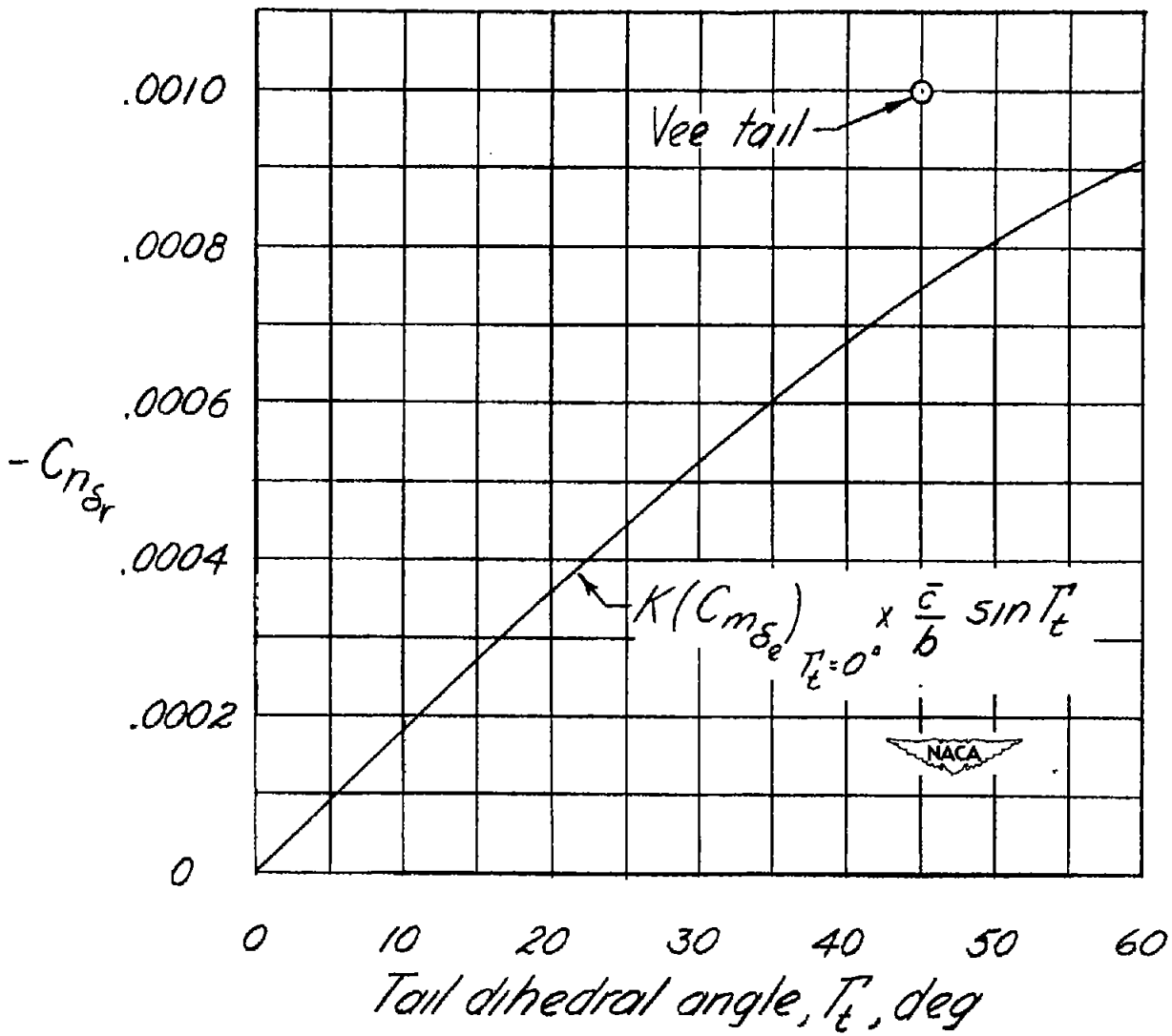

Figure 16.- Effect of tail dihedral angle on $C_{n_{\delta_r}}$.

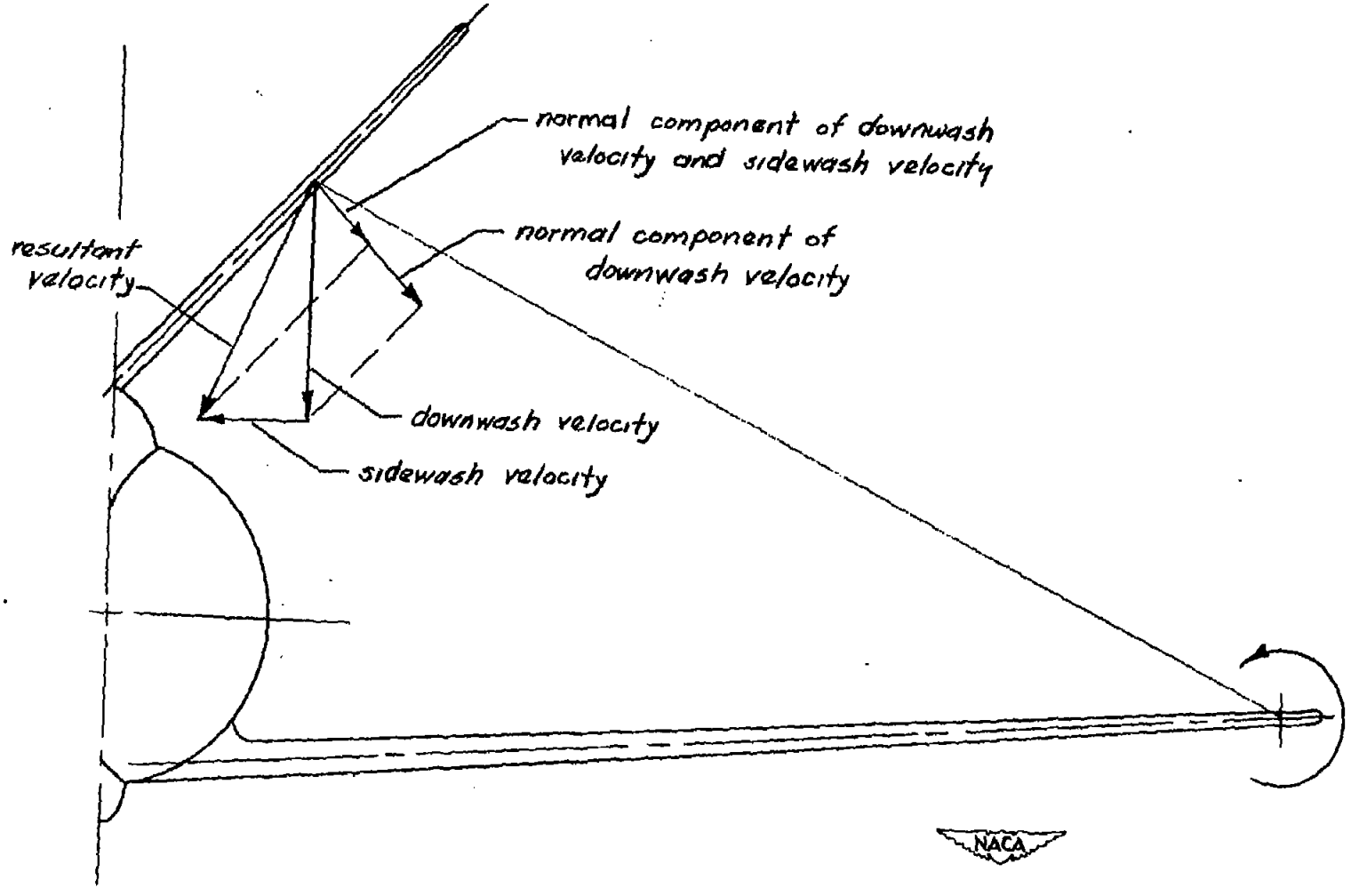

Figure 17.- Effect of sidewash on the induced velocity in the plane normal to the chord plane of the vee tail.